Comparison of cubic B-spline and Zernike-fitting techniques in complex wavefront reconstruction

M. Ares and S. Royo

We analyze an alternative to classical Zernike fitting based on the cubic B-spline model, and compare the strengths and weaknesses of each representation over a set of different wavefronts that cover a wide range of shape complexity. The results obtained show that a Zernike low-degree polynomial expansion or a cubic B-spline with a low number of breakpoints are the best choices for fitting simple wavefronts, whereas the cubic B-spline approach performs much better when more complex wavefronts are involved. The effect of noise level in the fit quality for the different wavefronts is also studied. © 2006 Optical Society of America

OCIS codes: 120.0120, 120.3940, 120.6650, 220.4840.

1. Introduction

The last step in the optical wavefront sensing train is the reconstruction of the wavefront surface from sampled measurements that have been taken using different techniques and under different conditions.[1] Reconstruction algorithms can basically be categorized as being either zonal or modal.[2] The modal approach involves data approximation in the whole domain using a polynomial function, whereas in the zonal model each reconstructed wavefront value is estimated just from its spatial neighbors' data.

The modal Zernike representation has been commonly chosen for wavefront fitting purposes. Its advantages range from its simple analytical form to the orthogonality of the basis in a continuous domain; moreover, its low-order terms are directly related to classical Seidel aberrations. However, Zernike polynomials have intrinsic limitations when complex wavefronts are involved. It has been shown that surfaces with multipeak and multihole shapes require flexible zonal approaches for satisfactory reconstruction.[3] Up to now, these surfaces have not been particularly relevant in optical testing, although complex wavefront generation from new optical elements such as deformable mirrors[4] and liquid-crystal spatial light modulators[5,6] has lately become possible. Thus the relevance of analyzing alternatives for the proper fitting of the new complex-shaped wavefronts is evident.

B-spline polynomials are especially well suited for this purpose. Recently, Liu and Gao[7] and Seifert *et al.*[8] pointed out their usefulness in different reconstruction schemes. B-splines have the advantage of being locally defined, of being fitted to the wavefront through well-known least-squares procedures, and of having great flexibility that allow their smoothness and polynomial degree to be controlled. Moreover, they are a commonly used description in optical element manufacture as far as computerized numerically controlled (CNC) grinding and polishing tools are easily commanded using it. To reach a high quality in optics manufacture through the newest technologies, iterative polishing steps using the surface measurement information are performed. However, the tested wavefront is not usually described on the same basis when it is measured and when it is used to control the polishing machine, which would obviously be the optimum scheme for industrial production.

The goal of this paper is to analyze the zonal cubic B-spline fitting method as an alternative to the modal Zernike technique when complex wavefronts are involved or whenever local control parameters are needed in the wavefront description. Sampled wavefronts from surfaces of increased complexity are simulated, and the quality of their fitted representations using Zernike and B-spline methods is compared. An

The authors are with The Center for Sensor, Instrumentation and System Development, Technical University of Catalonia (CD6-UPC), Rambla Sant Nebridi 10, Terrassa 08222, Spain. M. Ares's e-mail address is miguel.ares@oo.upc.edu and S. Royo's e-mail address is royo@oo.upc.edu.

Received 8 March 2006; accepted 3 May 2006; posted 16 May 2006 (Doc. ID 68675).

0003-6935/06/276954-11$15.00/0

analysis of the effects of noise level in each case is also performed.

This paper is organized as follows: In Section 2, a short theoretical review of the two fitting techniques is presented. Section 3 shows the reconstruction results attained by the Zernike and cubic B-spline techniques when they are applied to fit simple and increasingly more complex-shaped wavefronts. Finally, in Section 4, we summarize the main conclusions of the work.

2. Fitting Techniques

A brief mathematical review of the two fitting techniques analyzed will enable us to introduce the wavefront reconstruction principles on which they operate. The main theoretical concepts involved in both representations are presented next.

A. Three-Dimensional Zernike-Fitting Technique

Zernike circular polynomials were developed as a convenient set for representing a wavefront over a circular pupil. In addition to their simple analytical form, which makes them more practical than other polynomial sets (such as Karhunen–Loeve polynomials, for instance), Zernike modes can easily be related, in their lower orders, to classical Seidel aberrations such as spherical aberration, astigmatism, and coma.[9] The main advantages of the Zernike representation are afforded by the orthogonality of its modes over the unit circle. This means the aberration coefficient of each of the modes is linearly independent of the remaining ones, and also that the wavefront mean-square deviation (understood as its deviation from a known surface) is the sum of the mean-square deviation of individual modes. However, orthogonality is only achieved in the theoretical case of the description of a continuous surface. As far as real-world wavefront sampling gets discrete data, only good approximations of the last two properties are attained.

Several different notations for Zernike polynomials are to be found in the literature. In our work, we have followed the notation described by Malacara and DeVore.[9] As a complete modal set, any wavefront can be expressed as a linear combination of circular Zernike polynomials as follows:

$$W(\rho,\ \vartheta) = \sum_{n=0}^{k}\sum_{m=0}^{n} a_{nm} Z_n^{\,l}(\rho,\ \vartheta) = \sum_{i=1}^{L} a_i Z_i(\rho,\ \vartheta),$$
$$l = n - 2m, \tag{1}$$

where each basic polynomial function can be expressed as the product of a radial and an angular component,

$$Z_n^{\,l}(\rho,\ \vartheta) = \begin{cases} R_n^{\,l}(\rho)\cos(l\vartheta) & \text{for } l \le 0, \\ R_n^{\,l}(\rho)\sin(l\vartheta) & \text{for } l > 0, \end{cases} \tag{2}$$

where

$$R_n^{\,l}(\rho) = R_n^{\,n-2m}(\rho) = \sum_{s=0}^{m} (-1)^s \frac{(n-s)!}{s!\,(m-s)!\,(n-m-s)!}\,\rho^{n-2s}, \tag{3}$$

with polar unit circle data coordinates $0 \le \rho \le 1$, $0 \le \vartheta \le 2\pi$.

The values of the parameters involved in the description determine the polynomial fitting function. The main one is k, which is the Zernike *polynomial degree* selected, and the remaining ones are easily related to it. The n value ranges from 0 to k in unitary steps, fixing the degree of the radial component. For each n value, l varies between $-n$ and n in two unitary steps, fixing the azimuthal frequency of the angular component. Thus, both parameters determine each $Z_n^{\,l}$ Zernike mode. The number L of Zernike modes that compose the polynomial fitting function for a given degree k is defined by

$$L = \frac{(k+1)(k+2)}{2}. \tag{4}$$

Equation (1) shows the global fitting principle of the Zernike representation; that is, the data $W(\rho, \vartheta)$ are approximated by a polynomial function of degree k extended over the whole domain. Given N discrete data points from the measured wavefront $W_r(\rho_r, \vartheta_r)$ $r = 1, 2, \ldots, N$, where (ρ_r, ϑ_r) are the normalized 2D polar data coordinates, the only unknown parameters in Eq. (1) are the Zernike coefficients a_i. Obtaining the best estimation of those parameters means solving the linear least-squares problem described by the system of Eq. (1), which is written matricially as

$$Za = W, \tag{5}$$

or in detail:

$$\begin{bmatrix} Z_1(\rho_1,\ \vartheta_1) & Z_2(\rho_1,\ \vartheta_1) & \cdots & \cdots & Z_L(\rho_1,\ \vartheta_1) \\ Z_1(\rho_2,\ \vartheta_2) & Z_2(\rho_2,\ \vartheta_2) & \cdots & \cdots & Z_L(\rho_2,\ \vartheta_2) \\ \vdots & \ddots & \ddots & \ddots & \vdots \\ \vdots & \ddots & \ddots & \ddots & \vdots \\ \vdots & \ddots & \ddots & \ddots & \vdots \\ \vdots & \cdots & \ddots & \ddots & \vdots \\ Z_1(\rho_N,\ \vartheta_N) & Z_2(\rho_N,\ \vartheta_N) & \cdots & \cdots & Z_L(\rho_N,\ \vartheta_N) \end{bmatrix} \begin{bmatrix} a_1 \\ a_2 \\ \vdots \\ \vdots \\ a_L \end{bmatrix} = \begin{bmatrix} W(\rho_1,\ \vartheta_1) \\ W(\rho_2,\ \vartheta_2) \\ \vdots \\ \vdots \\ \vdots \\ W(\rho_N,\ \vartheta_N) \end{bmatrix}, \tag{6}$$

where W is the $N \times 1$ data matrix containing the sampled wavefront values, a is the $L \times 1$ matrix containing the Zernike coefficients to be determined,

and Z is the $N \times L$ matrix containing the values of the Zernike polynomials at each sampling point.

B. Three-Dimensional B-Spline-Fitting Technique

B-spline is a specific formulation for smooth surface generation, which follows general spline principles.[10] Any smooth piecewise polynomial function is called a spline. The principle is to divide the function domain into small enough subareas, in such a fashion that, in each subarea, a polynomial of relatively low degree can provide a good approximation to the surface data. Up to now, several different implementations of the B-spline surface model have been studied extensively. Perhaps, the simplest is the tensor product model,

$$W(x, y) = \sum_{i=0}^{n} \sum_{j=0}^{m} a_{ij} B_{i,k}(x) B_{j,l}(y), \tag{7}$$

where a_{ij} are the so-called control points, which act as subarea control parameters, and $B_{i,k}(x)$ and $B_{j,l}(y)$ are the ith and jth B-spline of degree $k - 1$ and $l - 1$ in the x and y directions, respectively. Equation (7) represents a wavefront as a linear combination of B-spline basic functions. Thus a formal similarity to the Zernike representation may be observed [see Eq. (1)], although no other similarity exists as the B-spline formulation will show.

For simplicity's sake, the discussion that follows deals only with the univariate x direction B-spline. No formulation difference exists in the bivariate case, as it is just the product of two separate univariates.

Three important user-selected parameters are involved in the B-spline representation

- The degree $k - 1$ of the B-spline.
- The number of breakpoints (NBP_x) that divide the domain into a set of subdomains ($x_{s=0}$, $x_{s=1}, \ldots, x_{s=\mathrm{NBP}_x-1}$).
- The smoothness level μ_s at break points: $\mu_s = 0$ means function discontinuity, $\mu_s = 1$ means function continuity, $\mu_s = 2$ means function and first derivative continuity, and so on.

Besides real NBP_x, the B-spline formulation creates the so-called knots t_i. Knots are fully coincident with breakpoints although, as knots, they may be repeated with a given multiplicity. The multiplicity of each knot is determined by the rule

$$\text{knot multiplicity}_s = k - \mu_s. \tag{8}$$

The nondecreasing knot set is formed by all the interior breakpoints repeated knot multiplicity times and the two end points of the domain repeated k times to account for the function discontinuity at the domain border. Although this last requirement can be relaxed, it has become standard. In knot notation, the set is described as $(t_0, t_1, t_2, \ldots, t_{n+k})$ where $n + 1$ is the number of control points, defined in Eq. (7). Taking into account the previous formulation, a practical relation gives the number of control points of a B-spline representation in terms of the three user-selected parameters,

$$n + 1 = \left(\sum_{s=1}^{\mathrm{NBP}_x - 2} k - \mu_s \right) + 2k - k. \tag{9}$$

As Eq. (7) shows, there are as many control points a_{ij} as there are B-spline functions. Each control point is a weight associated with each B-spline function, and has a local meaning because of the B-spline local support embedded in its definition.

The ith B-spline function of degree $k - 1$ is defined recursively as

$$B_{i,k}(x) = \frac{x - t_i}{t_{i+k-1} - t_i} B_{i,k-1}(x) + \frac{t_{i+k} - x}{t_{i+k} - t_{i+1}} B_{i+1,k-1}(x),$$

$$B_{i,1}(x) = \begin{cases} 1, & t_i \le x \le t_{i+1}, \\ 0, & \text{otherwise.} \end{cases} \tag{10}$$

Thus the ith B-spline function is the sum of k polynomials of degree $k - 1$ over the knot subinterval $(t_i, t_{i+1}, \ldots, t_{i+k})$. Outside that interval, the function is zero. The zeroth B-spline support is $(t_0, t_1, \ldots, t_k)$, the first B-spline support is $(t_1, t_2, \ldots, t_{1+k})$, and so on up to the nth B-spline, which is defined over $(t_n, t_{n+1}, \ldots, t_{n+k})$.

With reference to the particular B-spline scheme, we have applied to wavefront reconstruction; we have fixed $k = l = 4$ (cubic B-spline functions) and $\mu = 3$ (B-spline continuity up to the second derivative at all interior breakpoints). Thus we have left only NBP_x and NBP_y as free parameters. For simplicity's sake, we have also considered the same number of breakpoints in the x and y directions ($\mathrm{NBP}_x = \mathrm{NBP}_y$), which we herein refer to as NBP. In this particular situation, from Eq. (9) we can see that $n + 1 = m + 1 = \mathrm{NBP} + 2$.

To make the computational implementation simpler, we normalized the data coordinates x_r over each knot subinterval, taking values from 0 to 1,

$$tx_r = \frac{x_r - t_i}{t_{i+1} - t_i}, \quad x_r \in (t_i, t_{i+1}). \tag{11}$$

In this situation, the recursive B-spline description (10) becomes analytical. Thus each cubic B-spline function $B_{i,4}(tx)$ with support $(t_i, t_{i+1}, \ldots, t_{i+4})$ is described as follows (see Fig. 1),

$$B_{i,4}(tx) = B_{i,1}(tx) \cup B_{i+1,1}(tx) \cup B_{i+2,1}(tx) \cup B_{i+3,1}(tx), \tag{12}$$

where

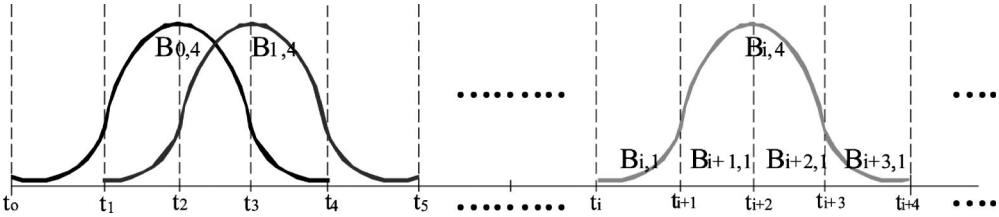

Fig. 1. Basic functions of the cubic B-spline representation along the fictitious knot domain.

$$
\begin{aligned}
B_{i,1}(tx) &= \frac{tx^3}{6},\\
B_{i+1,1}(tx) &= \frac{1}{6}\left(1 + 3tx + 3tx^2 - 3tx^3\right),\\
B_{i+2,1}(tx) &= \frac{1}{6}\left(4 - 6tx^2 + 3tx^3\right),\\
B_{i+3,1}(tx) &= \frac{1}{6}(1 - tx)^3, \qquad tx \in [0,\ 1]. \quad (13)
\end{aligned}
$$

Returning to the bivariate cubic B-spline scheme and given N discrete data points from the measured wavefront $W_r(tx_r, ty_r)$ $r = 1, 2, \ldots, N$, the unknown parameters of the system of Eq. (7) are only the values of control points a_{ij}:

$$
\begin{bmatrix}
B_{0,4}(tx_1)B_{0,4}(ty_1) & B_{0,4}(tx_1)B_{1,4}(ty_1) & \cdots & B_{n,4}(tx_1)B_{m,4}(ty_1)\\
B_{0,4}(tx_2)B_{0,4}(ty_2) & B_{0,4}(tx_2)B_{1,4}(ty_2) & \cdots & B_{n,4}(tx_2)B_{m,4}(ty_2)\\
\vdots & \ddots & \ddots & \vdots\\
\vdots & \ddots & \ddots & \vdots\\
\vdots & \ddots & \ddots & \vdots\\
\vdots & \cdots & \ddots & \vdots\\
B_{0,4}(tx_N)B_{0,4}(ty_N) & B_{0,4}(tx_N)B_{1,4}(ty_N) & \cdots & B_{n,4}(tx_N)B_{m,4}(ty_N)
\end{bmatrix}
\begin{bmatrix} a_{00}\\ a_{01}\\ \vdots\\ \vdots\\ \vdots\\ a_{nm} \end{bmatrix}
=
\begin{bmatrix} W(tx_1,\ ty_1)\\ W(tx_2,\ ty_2)\\ \vdots\\ \vdots\\ \vdots\\ W(tx_N,\ ty_N) \end{bmatrix}. \quad (14)
$$

As in the case of the Zernike basis, solving the linear least-squares problem described in Eq. (14) yields the best control point values for performing the wavefront reconstruction. In contrast to the Zernike case, most of the terms of the B-spline matrix are now zero as a consequence of the B-spline's local support.

3. Reconstruction Results

To study the capabilities of the cubic B-spline and Zernike-fitting methods when they are applied to different surface types, three sampled theoretical wavefronts of increasing complexity were generated. The simplest one—a spherical wavefront—and a more complex nonrotationally symmetrical sample—a toroidal wavefront—were simulated with analog characteristics to two wavefronts experimentally measured with an optical metrology setup based on the Ronchi test principle.[11,12] Besides its large dynamic range, the main advantage of the sensor arrangement is the extremely high wavefront sampling performance that is achieved using the microstepping technique,[11] so we will deal with sampled wavefronts with high-spatial resolution in the reconstruction analysis.

To complete the fitting analysis, we chose a decentered double-peak surface with a single hole, which has been extensively used by researchers to test new fitting schemes,[3] as a highly complex wavefront.

For the purposes of evaluating the Zernike and cubic B-spline representations, different polynomial degrees and NBP, respectively, were considered for the fit over the three selected wavefronts. However, there is an inherent difficulty in finding an appropriate comparison scheme due to the different reconstruction principles of both approaches. To give the reader a clear visual comparison of the two fitting techniques in the same plot, we have chosen to simultaneously plot the Zernike polynomial degree and the NBP value used for the B-spline approach along the horizontal axis, although they have different meanings in each case. It should be noted that NBP actually means NBP × NBP.

The comparison is carried out using two complementary quality fitting indicators: the rms wavefront deviation, which is defined as the rms difference between the reconstructed and ideal theoretical wavefronts, and the rms fit deviation, which gives the rms difference value between the measured and reconstructed wavefronts.

A. Zernike III Conditioning

To obtain the fitting solution for the Zernike and cubic B-spline representations, we used a powerful matrix inversion method called singular value decomposition (SVD).[13,14] Despite its higher computational cost[13] ($mn^2 + 5n^3/3 + 4n^3$ operations, m and n being the number of matrix rows and columns, respectively) in comparison to other methods such as

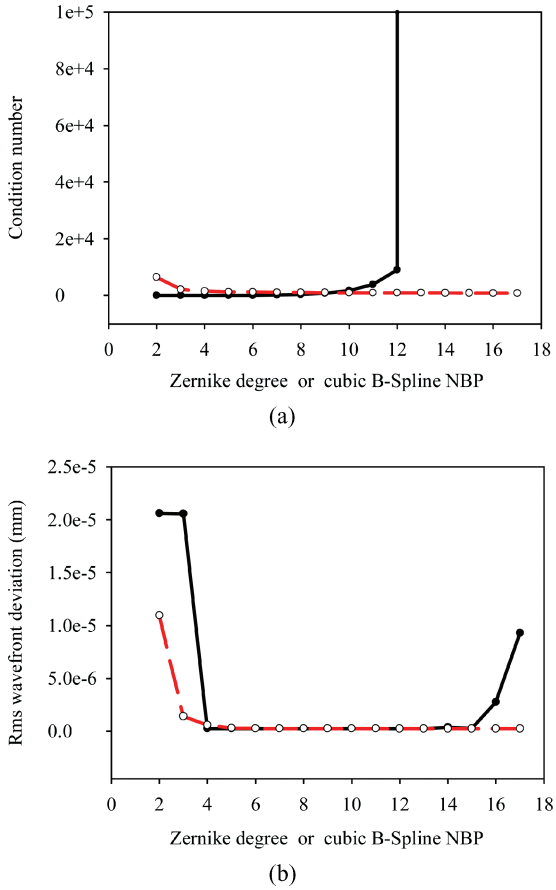

Fig. 2. (Color online) Zernike ill conditioning at high polynomial degrees (solid curve) for the ideal spherical wavefront, which is not present in any cubic B-spline scheme (dashed curve): (a) From the 13th degree, the Zernike matrix becomes singular, (b) which degrades the least-squares fitting solution obtained.

Cholesky or QR decompositions, the SVD method can always provide an unique solution even when the matrix moves away its full rank. This rank deficiency may be diagnosed through the so-called condition number, which is defined as the ratio of the largest to the smallest eigenvalue of the diagonal matrix of the decomposition. When the condition number is too large, the original matrix is singular or close to the singularity, and SVD provides a bad least-squares solution.

Figure 2(a) shows the condition number for the spherical wavefront case under the different Zernike degree and cubic B-spline NBP values. It should be noted that the same behavior was observed for the toroidal and the highly complex wavefronts, showing that it is independent of wavefront shape. The Zernike least-squares problem becomes poorly conditioned at high degree values, a fact which degrades the solution obtained [see Fig. 2(b)]. However, such degradation could be avoided along the decomposition process by simply zeroing the reciprocals of the eigenvalues of the diagonal matrix under a given threshold value,[14] although it stays up to the user to decide which is the proper threshold.

Table 1 presents the rms wavefront deviation, the condition number, and the values of the larger Zernike coefficients obtained for the degraded degree = 17 case before and after zeroing. Choosing an appropriate threshold improves the quality of the reconstruction (lower rms wavefront deviation), although the correct Zernike coefficient values are not obtained, if compared with the non-ill-conditioned degree schemes (anyone up to the 12th degree). While for those non-ill-conditioned schemes, the Zernike degree = $k + 1$ description maintains the values of the common coefficients with the degree = k description and even improves the quality of the reconstruction slightly by contributing new higher-order coefficients, for the zeroing modification the improvement is not accompanied by a correct aberration coefficient solution. High-degree Zernike reconstructions must therefore be disregarded, as we will do in the remainder of this paper. It should be stressed that this ill-conditioned problem does not appear in any of the B-spline cases, as shown by the dashed-line plot in Fig. 2(a).

B. Spherical Wavefront Reconstruction

As the simplest wavefront case, a spherical wavefront with a radius of curvature of 160 mm sampled at 6561 discrete points within a 2.51 cm^2 domain was

Table 1. Spherical Wavefront Fitting Results[a]

	Degree = 17	Degree = 17	Degree = 17	Degree = 17	Degree = 5
	No Zeroing	$\gamma_{min} \geq \gamma_{max} \times 10^{-12}$[b]	$\gamma_{min} \geq \gamma_{max} \times 10^{-9}$[b]	$\gamma_{min} \geq \gamma_{max} \times 10^{-3}$[b]	No Zeroing
Rms wavefront deviation (mm)	9.28×10^{-6}	2.45×10^{-7}	2.45×10^{-7}	7.59×10^{-2}	2.48×10^{-7}
Condition number	4.97×10^{30}	6.15×10^{11}	6.28×10^{8}	796.78	32.01
Highest Zernike coefficients (mm)	$a[1] = -1272.80$	$a[0] = 6.33 \times 10^{-2}$	$a[0] = 5.69 \times 10^{-3}$	$a[0] = 1.84 \times 10^{-4}$	$a[0] = 3.62 \times 10^{-4}$
	$a[2] = 3283.75$	$a[1] = -3.28 \times 10^{-2}$	$a[1] = 1.82 \times 10^{-4}$	$a[4] = -8.20 \times 10^{-5}$	$a[1] = 5.01 \times 10^{-4}$
	$a[4] = -0.85$	$a[2] = -3.28 \times 10^{-2}$	$a[2] = 1.82 \times 10^{-4}$	$a[12] = -3.90 \times 10^{-5}$	$a[2] = 5.01 \times 10^{-4}$
	$a[6] = -2544.31$	$a[4] = 0.11$	$a[4] = -7.39 \times 10^{-3}$	$a[24] = 7.50 \times 10^{-5}$	$a[4] = -1.75 \times 10^{-2}$
	$a[7] = -1085.89$	$a[12] = 8.40 \times 10^{-2}$	$a[12] = 6.10 \times 10^{-3}$	$a[42] = 3.50 \times 10^{-5}$	$a[12] = -7.00 \times 10^{-6}$
	$a[15] = 2939.39$	$a[14] = 0.22$	$a[26] = -1.85 \times 10^{-3}$	$a[60] = -5.10 \times 10^{-5}$	a[other] = 0
	$a[35] = -104,337.77$	$a[29] = 0.10$	$a[42] = -1.39 \times 10^{-3}$	$a[114] = -6.88 \times 10^{-4}$	
	$a[78] = -2,114,683.63$	$a[34] = 0.10$		$a[116] = -8.31 \times 10^{-4}$	
	$a[167] = 82,928.17$			$a[148] = 4.06 \times 10^{-4}$	

[a]Results are for the Zernike degree = 17 ill-conditioned case and for the non-ill-conditioned degree = 5.
[b]Value of the zeroing threshold used in each case; the reciprocal of any eigenvalue γ below $\gamma_{max} \times$ threshold is set to zero.

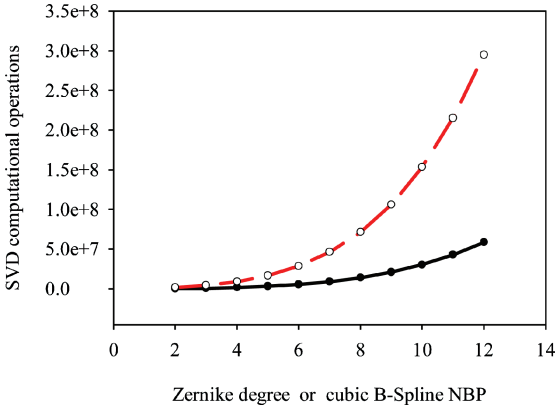

Fig. 3. (Color online) Number of computational operations involved in the SVD matrix inversion method for the different Zernike degrees (solid curve) and cubic B-spline NBP (dashed curve). An operation is a multiplication or a division plus an addition.

simulated. The fit quality as a function of the Zernike polynomial degree and the NBP for the cubic B-spline is depicted in the already mentioned Fig. 2(b). The results show that the Zernike method yields an excellent fitting quality for all non-ill-conditioned degree values from degree = 4. Below the fourth degree, the fit is not good enough, even with such a simple wavefront. As no higher-order aberrations terms are involved, the fourth-degree Zernike polynomial expansion is the optimum fitting scheme, as it avoids the more time-consuming computation of medium- to high-degree Zernike descriptions. The cubic B-spline representation attains a similar rms wavefront deviation as the Zernike from 6×6 NBP values (25 equally sized subareas), although not for lower ones. Moreover, B-spline calculation is more computationally intensive than the equivalent Zernike case. In this sense, Fig. 3 presents the comparison of the computational operations required to obtain the least-squares wavefront fitting solution under different degree–NBP values.

Having analyzed the two fitting techniques in the ideal wavefront, we now will deal with the effects of noise, as it occurs in real measurements. The spherical wavefront with random spatial noise added with relative values between $\pm 0.1\%$ of wavefront height peak to valley (PV), $\pm 0.5\%$ PV, and $\pm 1\%$ PV was simulated and fitted. Figures 4(a)–4(c) show the rms wavefront deviation and the rms fit deviation for the Zernike and cubic B-spline descriptions. In all cases, it can clearly be seen that the quality of the fit worsens for medium- to high-degree–NBP values, because in such cases, the fit follows the undesirable noise contributions better. That behavior is indicated not only by an increase in the rms wavefront deviation values, but also by a decrease in the rms fit deviation below the horizontal reference line that represents the rms deviation between the ideal and noisy wavefronts. In fact, the rms fit deviation only has meaning as an indicator for the quality of the fit if the noise amplitude is either well known, as in our theoretical study, or well estimated in experimental cases. Root-

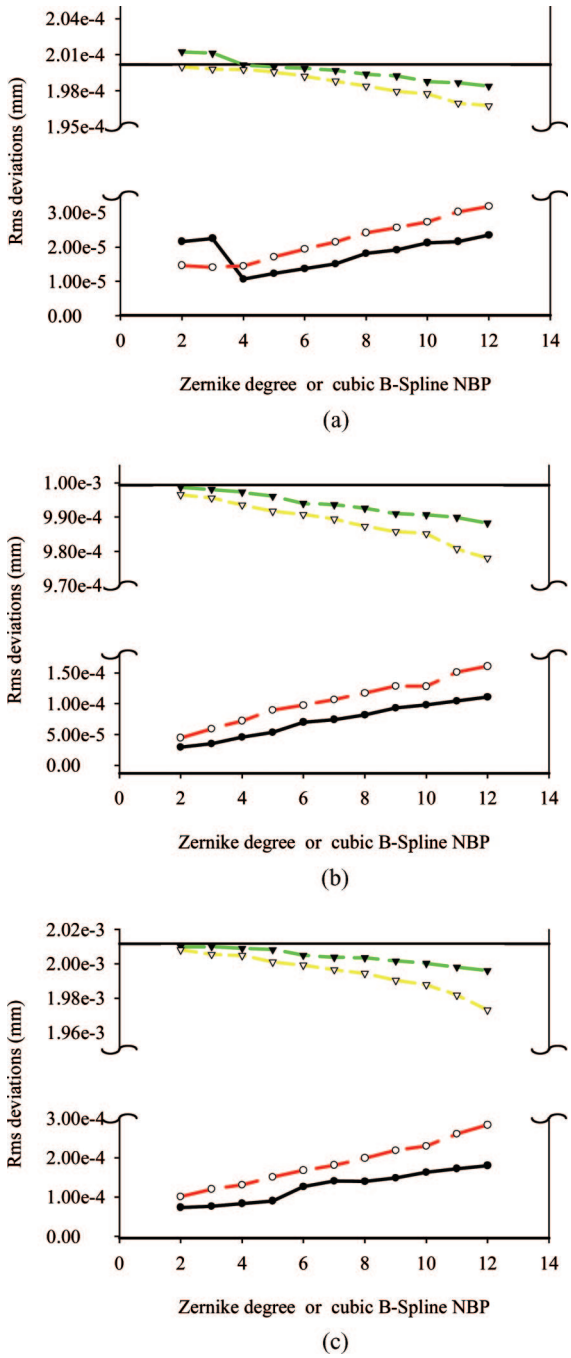

Fig. 4. (Color online) rms wavefront deviation (bottom, circles) and rms fit deviation (top, triangles) depending on the Zernike fit degree (filled symbols) and on the cubic B-spline NBP (nonfilled symbols), for the simulated noisy spherical wavefront. The upper horizontal reference line reflects the calculated rms deviation between the ideal and noisy wavefronts. (a) Noise amplitude between $\pm 0.1\%$ wavefront PV, (b) $\pm 0.5\%$ PV, and (c) $\pm 1\%$ PV.

mean-square fit deviation values above the reference line mean reconstructed wavefronts, which neither follow the noise nor accurately describe the wavefront shape, while rms fit deviation values below the line are associated with reconstructed wavefronts that follow the noise.

Meanwhile, the rms wavefront deviation is an ab-

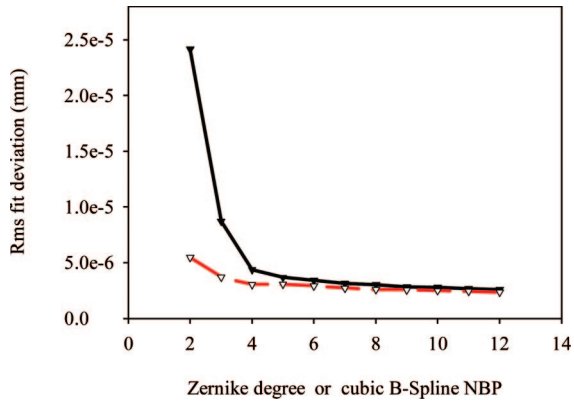

Fig. 5. (Color online) rms fit deviation for a spherical wavefront measured with a digital Ronchi test setup, under the different Zernike (solid curve) and cubic B-spline conditions (dashed curve).

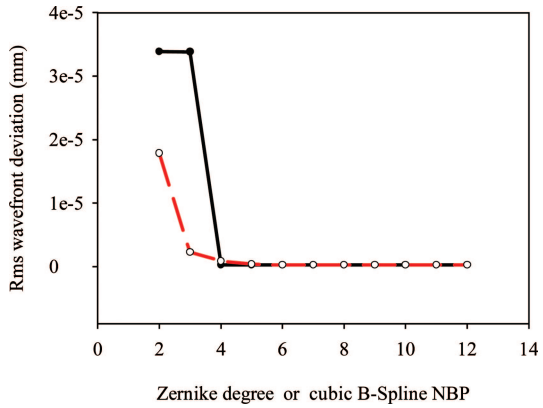

Fig. 6. (Color online) Zernike (solid curve) and cubic B-spline (dashed curve) rms wavefront deviation for the ideal toroidal wavefront rotated 30°.

solute indicator of reconstruction quality, although it has the serious lack that it is unknown for experimental wavefront fittings. Thus we understand that both rms parameters must be considered as useful complementary information to perform a quality fitting analysis.

Figure 4(a) shows that the best fitting scheme is the Zernike polynomial expansion of degree = 4. A very good rms wavefront deviation of 1.06×10^{-5} mm is obtained. Moreover, as expected, its rms fit deviation value (2.002×10^{-4} mm) is the closest one to the reference line value (2.007×10^{-4} mm). Zernike degree = 5 and even degree = 6 also provide a good fit. When the amplitude of the noise increases, the most noticeable fact is that the rms wavefront deviation tends to a strictly ascending line. For the ±0.5% PV and ±1% PV cases, the lowest degree = 2 (first six modes of the Zernike expansion) is the best scheme, as Figs. 4(b) and 4(c) show. Its rms fit deviations are the closest to the horizontal reference lines 9.99×10^{-4} mm and 2.01×10^{-3} mm, respectively. The cubic B-spline reconstruction is good for low NBP values (2×2 or 3×3), although its performance is not as excellent as that of the Zernike approach.

Finally, we performed the fitting analysis of real wavefronts measured using a digital Ronchi test setup. Although the Ronchi sensor directly measures the wavefront slopes at each sampled point, a simple integration algorithm calculates the corresponding height values.[12] However, the measurements are still discrete, so an accurate continuous wavefront representation is needed. A spherical wavefront obtained from the reflection of a point source in the concave surface of a spherical ophthalmic lens was fitted to the Zernike and cubic B-spline representations. The 6572 discrete data wavefront was defined within a 2.45 cm^2 domain. Figure 5 presents the rms fit deviation for the Zernike and cubic B-spline descriptions. The really low rms values obtained (a factor almost 100 smaller than the ±0.1% PV noise case) tell us that the amount of noise present in the wavefront is negligible; therefore, the best reconstruction setting is the Zernike degree = 4 representation as suggested by the theoretical results.

C. Toroidal Wavefront Reconstruction

A toroidal wavefront with a sampling of 6084 data on a 3.16 cm^2 domain was simulated on the basis of the most general spherocylindrical surface equation mathematically described as

$$x - x_0 = x_r \cos \vartheta + y_r \sin \vartheta,$$

$$y - y_0 = -x_r \sin \vartheta + y_r \cos \vartheta,$$

$$z = \frac{(x - x_0)^2/R_1 + (y - y_0)^2/R_2}{1 + \left\{1 - \frac{[(x - x_0)^2/R_1 + (y - y_0)^2/R_2]^2}{(x - x_0)^2 + (y - y_0)^2}\right\}^{1/2}}. \quad (15)$$

A rotation of $\vartheta = 30°$ from the x and y reference axes and a radii of curvature $R_1 = 150$ mm and $R_2 = 170$ mm of the principal meridians were selected for the surface. With those radii values and the domain region used, the spherocylindrical surface may be considered to be fully equivalent to the toroidal surface.[12]

As for the spherical case, the fit quality is once again evaluated for the different Zernike degrees and cubic B-spline NBP values. As Fig. 6 shows, the same quality behavior of the case of the spherical wavefront is obtained.

Unfortunately, real wavefronts are not ideal, and the quality of both fitting techniques must be analyzed in noisy conditions. The same toroidal wavefront was simulated with a spatial random noise distribution with values between ±0.1% of wavefront PV, ±0.5% PV, and ±1% PV. For the lowest amount of noise considered, the rms deviations almost have the same behavior as for the spherical case. The optimum fitting scheme is again the Zernike polynomial expansion of degree = 4, and really close to it we find the NBP = 3×3 cubic B-spline description [see

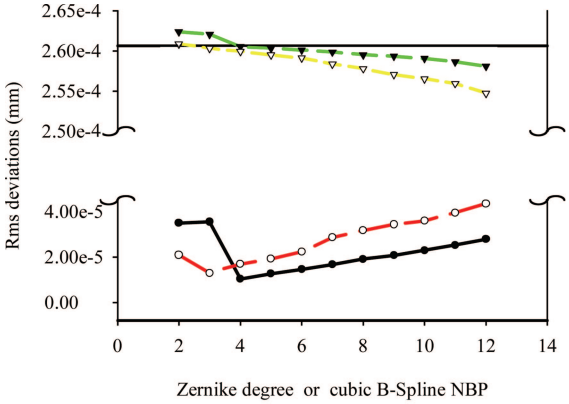

(a)

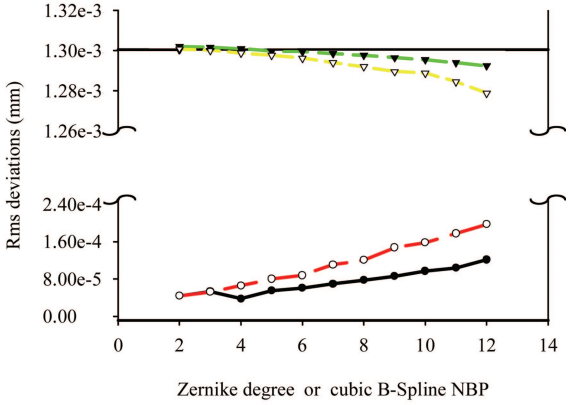

(b)

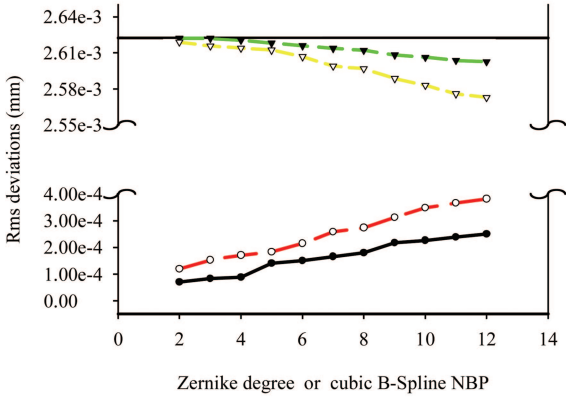

(c)

Fig. 7. (Color online) rms wavefront deviation (bottom, circles) and rms fit deviation (top, triangles) depending on the Zernike fit degree (filled symbols) and on the cubic B-spline NBP (nonfilled symbols), for the simulated noisy toroidal wavefront. The upper horizontal reference line reflects the calculated rms deviation between the ideal and noisy wavefronts. (a) Noise amplitude between ±0.1% wavefront PV, (b) ±0.5% PV, and (c) ±1% PV.

Fig. 7(a)]. Despite the close similarity, for the toroidal case it can be seen that the quality reconstruction for schemes below the optimum ones (i.e., degree = 2 and 3, NBP = 2 × 2) is worse than for the spherical wavefront case. This is a consequence of the more complex toroidal shape, which even more forcefully

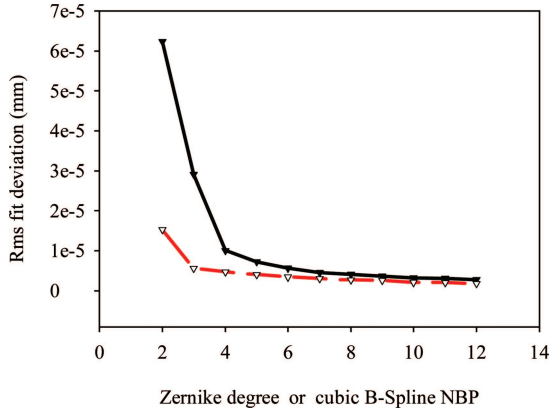

Fig. 8. (Color online) rms fit deviation of the Zernike (solid curve) and cubic B-spline (dashed curve) representations for the experimental rotated toroidal wavefront.

suggests disregarding the lowest-order fitting approaches.

As for the spherical wavefront, when the noise amplitude is increased, the problem of noise following in the fitted data becomes a more critical issue. Thus the lowest degree–NBP scheme is again preferable, as Fig. 7(c) shows. However, for the toroidal ±0.5% PV case, the Zernike degree = 4 already yields the optimum fit, in contrast with the spherical, for which degree = 2 performed better. Once again, it is the slightly more complex shape of the toroidal wavefront that accounts for this fact.

Finally, we applied the Zernike and cubic B-spline representation techniques to an experimental toroidal wavefront measured with the Ronchi sensor. The 6125 discrete data toroidal sample was defined within a 2.80 cm^2 area, and its principal meridians were rotated 30° from the *xy* reference axes (in similarity with the simulated toroidal wavefront). As expected, the same rms fit deviation behavior found in the real spherical wavefront was obtained (Fig. 8). Again, the very low rms values confirm that the measured wavefront is almost noiseless; therefore the Zernike degree = 4 polynomial is the best fitting option.

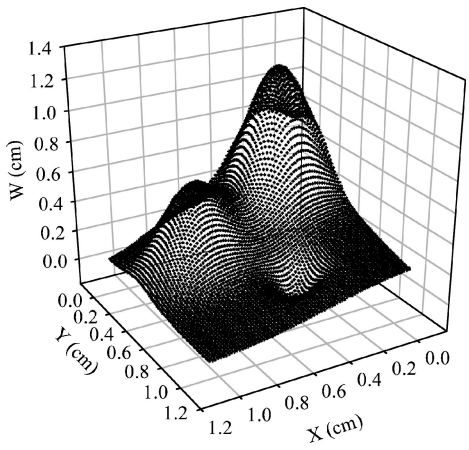

Fig. 9. Highly complex wavefront selected.

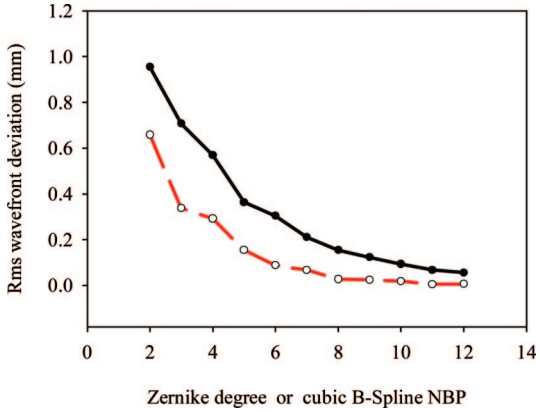

Fig. 10. (Color online) rms wavefront deviation for the ideal highly complex wavefront under different Zernike degree (solid curve) and cubic B-spline NBP (dashed curve) cases.

D. Complex Wavefront Reconstruction

As a highly complex wavefront, we chose a decentered double-peak surface with a single hole, historically known as Franke's function, defined over the domain $x \in [0, 1.1]$ cm $y \in [0, 1.1]$ cm (see Fig. 9).[3] The fit quality is obtained again for different Zernike degree and B-spline NBP conditions. As shown in Fig. 10, neither the low Zernike degrees nor the cubic B-spline low NBP can reproduce the complex wavefront shape with accuracy. High-degree Zernike representations are also invalid due to ill conditioning (see Subsection 3.A). Although in both representations, the rms wavefront deviation decreases when the degree or NBP increases, the cubic B-spline yields a better fit of the highly complex wavefront. The lowest rms wavefront deviation values are achieved in the B-spline's high NBP zone. These values are not reached by any of the Zernike functions.

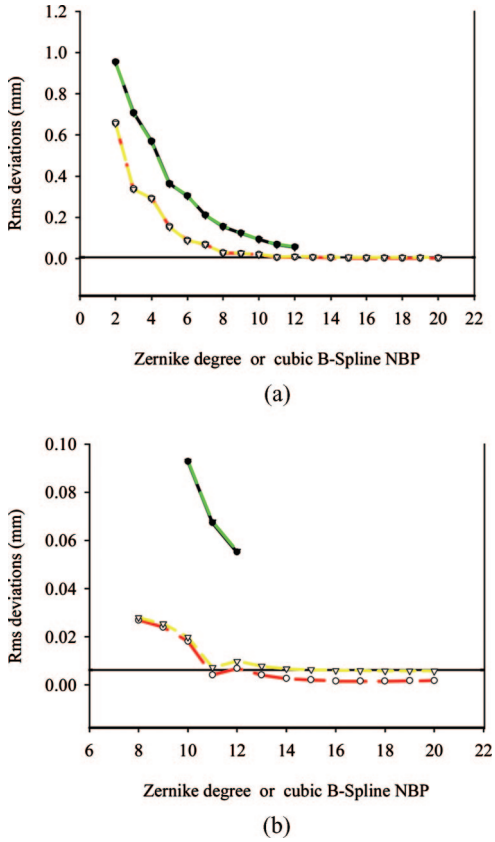

Fig. 11. (Color online) Comparison of Zernike (top) and cubic B-spline (bottom) rms wavefront deviation (circles) and rms fit deviation (triangles) for the highly complex wavefront with random noise added between ±0.1% wavefront PV. The horizontal reference line reflects the calculated rms deviation between the ideal and noisy wavefronts. (a) Low-degree–NBP schemes do not reproduce the complex shape at all, and (b) the appropriate working zone, in which the cubic B-spline performs better than the Zernike (NBP = 16 × 16 is the optimum fit).

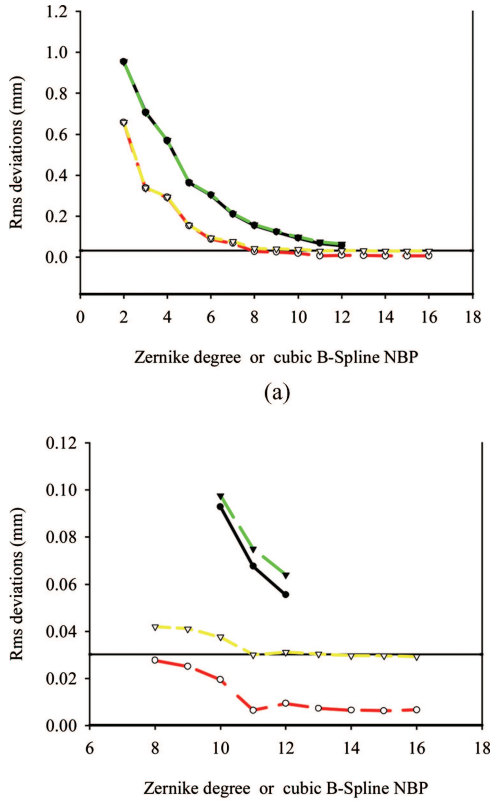

Fig. 12. (Color online) Comparison of Zernike (top) and cubic B-spline (bottom) rms wavefront deviation (circles) and rms fit deviation (triangles) for the highly complex wavefront with random noise added between ±0.5% wavefront PV. The horizontal reference line reflects the calculated rms deviation between the ideal and noisy wavefronts. (a) Low-degree–NBP fits do not follow the wavefront shape and (b) the appropriate working zone, which gives the NBP = 11 × 11 cubic B-spline as the best fit.

To analyze the fitting techniques in real conditions, a noise added situation was simulated for the highly complex wavefront, although no experimental sample of this case was available when this paper was being drafted. Again, the synthetic experimental highly complex wavefront was generated with a spatial random noise between ±0.1% of wavefront PV, ±0.5% PV, and ±1% PV. While for the spherical and toroidal wavefronts, low degree–NBP values were considered to be the best fitting solutions, Figs. 11(a),

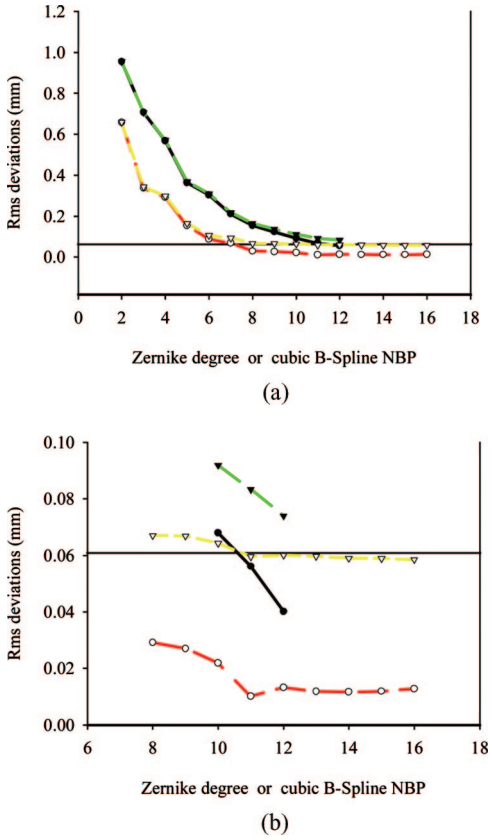

Fig. 13. (Color online) Comparison of Zernike (top) and cubic B-spline (bottom) rms wavefront deviation (circles) and rms fit deviation (triangles) for the highly complex wavefront with random noise added between ±1% wavefront PV. The horizontal reference line reflects the calculated rms deviation between the ideal and noisy wavefronts. (a) Low-degree–NBP fits do not follow the wavefront shape and (b) the appropriate working zone, in which NBP = 11 × 11 is the optimum fitting scheme.

12(a), and 13(a) show that low degree–NBP can not follow the complex wavefront shape at all. It is only from 8 × 8 NBP (49 equally sized subareas) for the cubic B-spline description that the complex surface shape starts to be reproduced quite accurately. The higher Zernike degree expansions also perform a good reconstruction, but they clearly do not attain the quality of the cubic B-spline. From Figs. 11(b), 12(b), and 13(b), it can be seen that B-spline rms wavefront deviation values are always lower than Zernike ones. For the ±0.1% PV case, the optimum fitting scheme is the NBP = 16 × 16 as an inflection point between complex shape reconstruction that is not particularly accurate (NBP values below 16 × 16) and noise following (NBP values above 16 × 16). When the amplitude of the noise increases, the inflection point goes down due to the need to reduce the local influence of the B-spline to prevent following the larger noise (as we also saw in the spherical and toroidal cases). The NBP = 11 × 11 is then the optimum fitting scheme in this case. This is, when a relevant amount of noise is present in the measurement, to reduce the noise-following effect by reducing the NBP value used should be considered.

4. Conclusions

The cubic B-spline fitting technique, which is an alternative to the classical Zernike polynomial expansion, was introduced and analyzed in detail. A comparison between the modal Zernike and the zonal cubic B-spline fitting methods was performed over wavefronts that cover a wide range of complexity, from the simplest case (spherical) to a highly complex wavefront.

The analysis was based on fit quality. In addition to the rms difference between the ideal and the reconstructed wavefront information—the rms wavefront deviation—we also pointed out the need to use the rms difference between the real and the reconstructed wavefront—the rms fit deviation—as a complementary quality indicator to deal with experimental wavefronts.

When the wavefront involved is simple, as spherical or even toroidal, a low-degree Zernike expansion, as well as a low NBP cubic B-spline, perform the optimum fitting. They accurately reproduce the wavefront shape without following the noise. The Zernike approach reaches the maximum quality and must be considered when direct aberration information is needed, whereas the cubic B-spline should be considered when local wavefront information knowledge is useful. In more complex wavefront fitting, however, the performance of the cubic B-spline technique is clearly superior to that of the Zernike fitting. Low-degree–NBP cannot reproduce the complex wavefront shape at all, and good quality reconstructions are only achieved in the medium- to high-degree–NBP zone. Despite the good quality of the Zernike reconstruction in high-degree conditions, the aberration coefficients solution obtained is not physically correct, although it is mathematically, and should be considered invalid. This is a consequence of the matrix representation's rank deficiency at high Zernike degrees, which is not present in any of the B-spline cases. The cubic B-spline description with a high NBP value performs much better in complex wavefront reconstruction. When noise is present, the optimum reconstruction scheme should reproduce the surface without following the noise, so the optimum NBP value will depend on the particular noise amplitude present in the measurement.

The authors thank the Spanish Ministry of Education and Science for the AP2003-3140 grant received and for the project DPI2005-00828, which has partially funded this research.

References

1. R. R. Rammage, D. R. Neal, and R. J. Copland, "Application of Shack–Hartmann wavefront sensing technology to transmissive optic metrology," *in Advanced Characterization Techniques for Optical, Semiconductor, and Data Storage Components,* A. Duparré and B. Singh, eds., Proc. SPIE **4779,** 161–172 (2002).
2. W. H. Southwell, "Wave-front estimation from wave-front slope measurements," J. Opt. Soc. Am. **70,** 998–1006 (1980).
3. K. W. Farmer, "Scattered data interpolation by C quintic

splines using energy minimization," M. A. thesis (University of Georgia, 1997).
4. G. Vdovin and P. M. Sarro, "Flexible mirror micromachined in silicon," Appl. Opt. **34,** 2968–2972 (1995).
5. P. M. Prieto, E. J. Fernández, S. Manzanera, and P. Artal, "Adaptive optics with a programmable phase modulator: applications in the human eye," Opt. Express **12,** 4059–4071 (2004).
6. L. Seifert, J. Liesener, and H. J. Tiziani, "The adaptive Shack–Hartmann sensor," Opt. Commun. **216,** 313–319 (2003).
7. X. Liu and Y. Gao, "B-spline based wavefront reconstruction for lateral shearing interferometric measurement of engineering surfaces," *Advances in Abrasive Technology V* (Trans Tech Publications, 2003), Vol. 238–239, pp. 169–174.
8. L. Seifert, H. J. Tiziani, and W. Osten, "Wavefront reconstruction with the adaptive Shack–Hartmann sensor," Opt. Commun. **245,** 255–269 (2005).
9. D. Malacara and S. L. DeVore, "Interferogram evaluation and wavefront fitting," in *Optical Shop Testing,* 2nd ed., D. Malacara, ed. (Wiley, 1992).
10. C. de Boor, *A Practical Guide to Splines,* revised edition (Springer-Verlag, 2001).
11. J. Arasa, S. Royo, and N. Tomás, "Simple method for improving the sampling in profile measurements by use of the Ronchi test," Appl. Opt. **39,** 4529–4534 (2000).
12. S. Royo, J. Arasa, and C. Pizarro, "Profilometry of toroidal surfaces with an improved Ronchi test," Appl. Opt. **39,** 5721–5731 (2000).
13. C. L. Lawson and R. J. Hanson, *Solving Least Square Problems* (Prentice Hall, 1974).
14. W. H. Press, S. A. Teukolsky, W. T. Vetterling, and B. P. Flannery, *Numerical Recipes in C,* 2nd ed. (Cambridge U. Press, 1997).